Variability of upwelling and chlorophyll in the equatorial Atlantic

Semyon A. Grodsky,[1] James A. Carton,[1] and Charles R. McClain[2]

Received 25 October 2007; revised 5 December 2007; accepted 2 January 2008; published 8 February 2008.

[1] The primary seasonal phytoplankton bloom in the equatorial Atlantic occurs in boreal summer in response to seasonal strengthening of zonal winds. However, the equatorial Atlantic also has a secondary bloom in late fall – early winter. This secondary bloom is weaker than the primary bloom by a factor of two, but is subject to year-to-year variability that is similar in magnitude. Here, observational evidence, including sea level and SeaWiFS-derived chlorophyll-a concentration, is used to examine several potential causes of this secondary bloom. The secondary bloom varies independently of blooms along the eastern coastal zones. Also, the secondary bloom has a relationship with the cessation of the Northwest African monsoon, which propotes the secondary seasonal strengthening of the trade winds. The variability of the secondary bloom results from perturbations in the depth of the thermocline induced by zonal wind anomalies in the western tropical Atlantic. These wind anomalies are correlated with mean sea level atmospheric pressure anomalies in the region of the northern subtropical high as well as over the Amazon. **Citation:** Grodsky, S. A., J. A. Carton, and C. R. McClain (2008), Variability of upwelling and chlorophyll in the equatorial Atlantic, *Geophys. Res. Lett.*, *35*, L03610, doi:10.1029/2007GL032466.

1. Introduction

[2] Along the equator, where solar radiation is not a limiting factor, chlorophyll-*a* (Chl-a) concentration reflects the strength of the nutrient flux into the mixed layer by equatorial upwelling [*Longhurst*, 1993]. In the equatorial Atlantic, the strength of upwelling varies seasonally with the strength of the zonal winds, weakening in early boreal spring and intensifying again in April–May. But, despite this well-defined seasonality of winds, there is some disagreement in the scientific literature on the seasonality of Chl-a. *Monger et al.* [1997] explored a year-long record for 1979 of Coastal Zone Color Scanner data and found that Chl-a peaked in late fall-early winter. In contrast, two years (1997–1998) of records from the Sea-viewing Wide Field-of-view Sensor (SeaWiFS) indicated a single summer-fall bloom in July–September [*Signorini et al.*, 1999]. *Perez et al.* [2005] revisited the seasonality of Chl-a using four years of SeaWiFS records finding that the primarily bloom does indeed occur in boreal summer in conjunction with strengthening zonal winds, but noted the existence of a secondary late-season bloom. In this paper we use an expanded 10 years of SeaWiFS records to examine both the seasonal cycle of Chl-a and its interannual variations while exploring their links to locally and remotely varying winds.

[3] Because changes in upwelling are reflected in SST as well as Chl-a, we begin by describing the seasonal cycle of equatorial SST. In July, SST in the east decreases to a cool 23.5°C between 20°W–5°E while temperatures warm further west (28.5°C at 45°W) in response to westward equatorial winds. *Perez et al.* [2005] found that in summer Chl-a reaches a maximum concentration of between 0.6 and 1.4 mg.m^{-3} at 0°N, 10°W with the higher values occurring in years of stronger upwelling.

[4] By September, the equatorial trade winds weaken and the sun approaches the equator, and, as a result, the tongue of cool SST in the eastern basin begins to warm such that, by October–November, SSTs are fairly uniform in the zonal direction. As originally observed in coastal time series [*Morliere and Rebert*, 1972], a weak secondary cooling follows about a month later, near the end of the calendar year, accompanied by a shoaling of thermocline in the Gulf of Guinea [*Schouten et al.*, 2005]. Although the SST anomaly associated with this shoaling is weak, its impact on Chl-a may be significant. In 2001, *Perez et al.* [2005] note a substantial 0.4 mg.m^{-3} increase in Chl-a concentration at 25°W–10°W from October to December despite only a weak <0.5°C cooling of SST. These observations raise the question of the relative importance of summer and winter blooms in the climatological seasonal cycle and their interannual variability. In addition, there are some alternative explanations regarding the cause of the secondary cooling of SST. *Philander and Pacanowski* [1986] suggest that it is forced remotely by the abrupt intensification of southeasterly wind in May–June and its delayed impact on the thermocline through equatorial waves, while *Okumura and Xie* [2006] suggest that it is a direct response of the ocean to instantaneous wind variations induced by changes in Amazonian convection.

[5] In this paper, we use an expanded set of remotely sensed observations to revisit the problem of the seasonal cycle of Chl-a along the equator, its relationship to the thermocline depth and SST, and its link to seasonal wind variations. Finally, we examine the interannual variability of Chl-a and connections to zonal wind variations over the western equatorial Atlantic.

2. Data

[6] This study relies heavily on a number of observational datasets, including satellite retrievals of ocean color, sea level, SST, and winds. The variability of the ocean color in the tropical Atlantic is analyzed using weekly averaged Chl-a on a 1/4° × 1/4° grid provided by the SeaWiFS project [*McClain et al.*, 2004]. Altimeter-based merged weekly sea

[1]Department of Atmospheric and Oceanic Science, University of Maryland at College Park, College Park, Maryland, USA.
[2]NASA Goddard Space Flight Center, Greenbelt, Maryland, USA.

0094-8276/08/2007GL032466

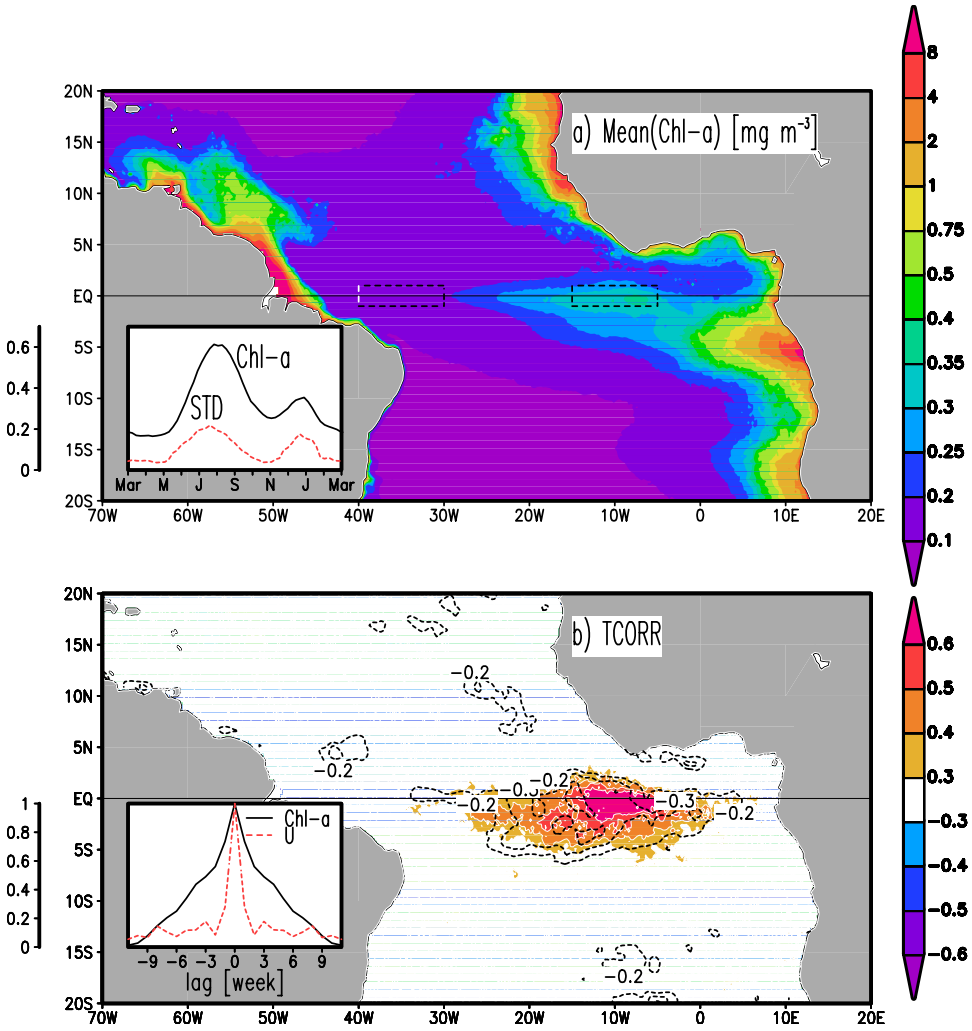

Figure 1. Statistics of Chl-a. (a) Time mean concentration based on 1997–2006 average. Inlay shows the seasonal cycle and the standard deviation (STD) about the seasonal cycle averaged in the eastern box. (b) Time correlation of anomalous Chl-a in the eastern box with anomalous Chl-a (shading) and SSH (contours). Inlay shows autocorrelations of anomalous Chl-a in the eastern box and zonal wind (U) in the western box.

surface height anomaly (SSH) is provided by the Archiving, Validation and Interpretation of Satellite Oceanographic data (AVISO) on a 1/3° × 1/3° grid [*Ducet et al.*, 2000]. In this discussion, SSH is used as a proxy for thermocline depth to which it is correlated, with correlations exceeding 0.85 [*Arnault et al.*, 1992]. The regression coefficient relating the two variables can be estimated by comparison with the moored time series of temperature at the 0°N, 0°W PIRATA mooring [*Servain et al.*, 1998]. Our comparison shows that a 5 cm decrease in SSH is associated with a 35 m shallowing of the 20°C isotherm.

[7] SST is provided by the Microwave Imager aboard the Tropical Rainfall Measuring Mission satellite and distributed by the Remote Sensing Systems. We use microwave rather than infrared SST because it is less affected by clouds. Near-surface ocean winds are provided by QuikSCAT scatterometry [*Liu*, 2002]. We obtain this data from the NASA/JPL where it has been converted to 10m neutral wind and mapped twice daily onto a 0.5 × 0.5° grid. All data are averaged weekly to match the temporal resolution of SSH. Atmospheric conditions are further characterized by the mean sea level pressure (MSLP) provided daily on a 2.5 × 2.5° grid by the NCEP/NCAR Reanalysis of *Kalnay et al.* [1996]. A weekly climatology is computed for each variable based on whatever fraction of our 10-year period 1997–2006 is available for the particular measurement. Weekly anomalies are then computed relative to that climatology, and the linear trend is subtracted.

3. Results

[8] The highest time mean Chl-a in the tropical Atlantic occurs in coastal and adjacent areas as a result of river discharge and coastal upwelling (Figure 1a). In the eastern tropical Atlantic, upwelling of nutrient rich waters produces Chl-a exceeding 0.5 mg.m^{-3} off Northwest Africa as well as the southern Benguella upwelling zone. Between the two, the Congo River plume is associated with a local maximum of Chl-a along 5°S. In the western tropical Atlantic, high Chl-a occurs within the Amazon and Orinoco River plumes. In contrast, Chl-a is low in the northeastern Gulf of Guinea despite the presence of the Niger and Volta Rivers. A

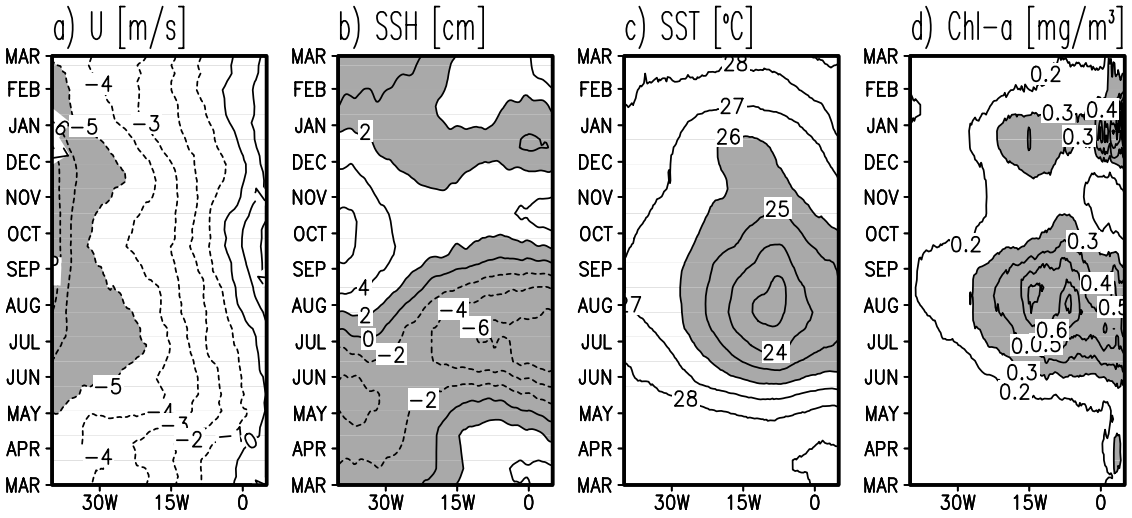

Figure 2. Seasonal cycle of equatorial (a) zonal winds (U), (b) SSH, (c) SST, and (d) Chl-a.

secondary maximum occurs along the equator, with values exceeding 0.35 mg.m^{-3} in the 20°–0°W band.

[9] In the interior ocean, the Chl-a increases gradually with decreasing latitude from the subtropical gyres toward the equator (Figure 1a). This meridional increase is linked to meridional changes of vertical motions from subduction in the subtropical gyres to upwelling along the equator. Thus, the seasonal cycle of Chl-a in the equatorial belt reflects seasonal variations of upwelling and equatorial zonal winds that follow the seasonal march of the Intertropical Convergence Zone (ITCZ). The seasonal peak of Chl-a on the equator occurs in boreal summer and reaches 0.6 mg.m^{-3} (Figure 1a, inlay) when the ITCZ is in its northernmost position and zonal winds over the equator are enhanced. A noticeable secondary late-season Chl-a bloom develops in December–January. Although the Chl-a concentration during the summer (primary) bloom exceeds that of the late-season (secondary) bloom by a factor of 2, the magnitude of anomalies is similar during both blooms.

[10] The semiannual cycle of Chl-a may be attributed to the season of maximum equatorial upwelling (boreal summer) and the season of maximum discharge from the Congo River (boreal winter) [*Gregg*, 2002]. However, a time correlation of anomalous Chl-a indicates coherent variations along the equator that occur independently of variations along the eastern coast (Figure 1b). This independent behavior is explained by a characteristic time scale of Chl-a loss (about a week [e.g., *Uz and Yoder*, 2004]) and a characteristic westward velocity in the South Equatorial Current (ranging from 10 to 30 cm.s^{-1}) that defines a characteristic advection length scale of less than 2°. However, the zonal scale of Chl-a correlation along the equator is around 30° (Figure 1b) and vastly exceeds the advection length scale. This broad correlation is produced by perturbations of equatorial upwelling by eastward propagating Kelvin waves [*Servain et al.*, 1982]. Perturbations of Chl-a along the equator occur coherently on spatial/temporal scales of 30° lon/3 weeks defined by transient Kelvin waves. This mechanism suggests a positive spatial correlation between Chl-a enhancement and thermocline shoaling as seen in Figure 1b.

[11] The temporal and longitudinal correspondence of seasonal Chl-a, SSH, SST, and winds along the equator is presented in Figure 2, essentially confirming the results of *Perez et al.* [2005]. Equatorial winds weaken in early boreal spring and then strengthen through June mainly in the west (Figure 2a). In response, the thermocline shoals dramatically in the east by June–July (Figure 2b). This shoaling increases entrainment of cold nutrient-rich water into the mixed layer (Figure 2c), leading to the Chl-a bloom in July–August (Figure 2d), which occurs in phase with cool SST. Beginning in July, zonal winds start weakening again. But, in November, the winds undergo a second seasonal strengthening as the Northwest African monsoon relaxes, increasing upwelling and uplifting the thermocline in the east, cooling SSTs somewhat, and inducing a second seasonal bloom.

[12] We next consider nonseasonal anomalies, which combine both intraseasonal and interannual variations, in an eastern equatorial box centered on the location of the seasonal maximum of Chl-a (15°W–5°W, 2°S–2°N, Figure 1). Variations of Chl-a and SSH in the east are compared with zonal winds in the west following *Servain et al.* [1982]. On both intraseasonal and interannual timescales, Chl-a and SSH (thus thermocline depth) are highly correlated with zonal winds (Figures 3a and 3b). Interestingly, the Chl-a and SSH contain a slow multi-year modulation that does not seem to be related to winds. In fact, low Chl-a/high SSH before 2000 was followed by high Chl-a/low SSH during 2000–2002. But this latter shoaling of the thermocline was not accompanied by strengthening of zonal winds that remained normal on average during 2000–2002. This discrepancy between multi-year variations of winds and thermocline depth can be forced remotely by *e.g.* the oceanic subtropical cells [*Schott et al.*, 2004]. These cells transport water subducted in the subtropics into the equatorial upwelling zones and thus affect the equatorial thermocline independently of local winds.

[13] The most dramatic anomalous shoaling of the thermocline occurs late in 2001, extending into the beginning of 2002 (Figure 3a). This shoaling also corresponds to the most dramatic secondary bloom in the 10-year record. It is

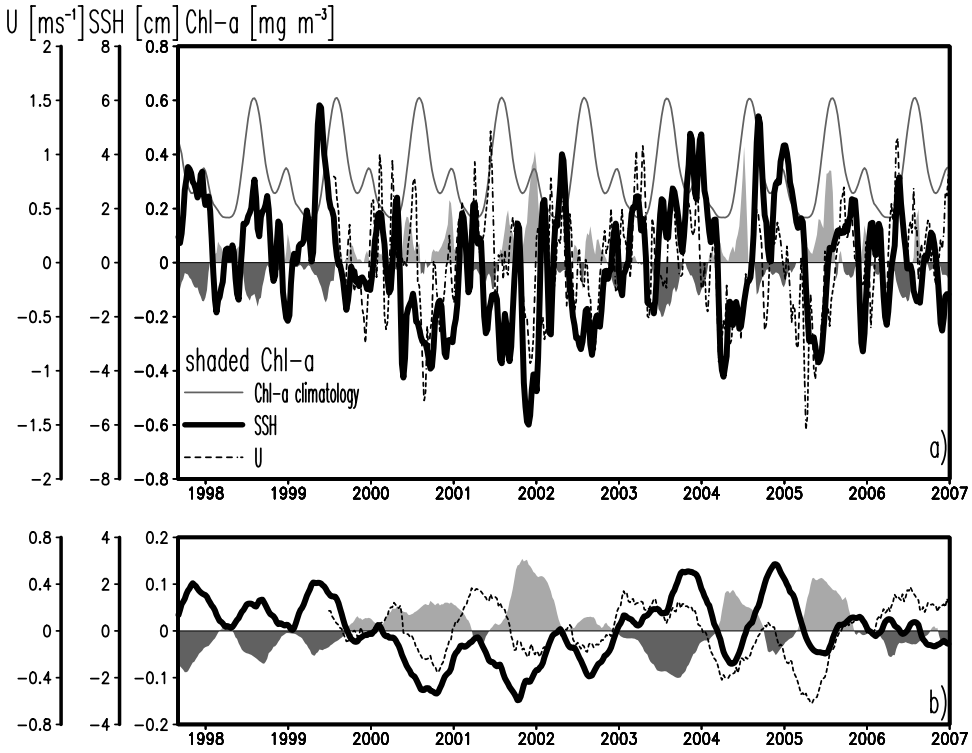

Figure 3. Time series of anomalous Chl-a and SSH in the eastern box, and zonal winds (U) in the western box. (a) Weekly averaged time series, (b) 27-week running mean. Weekly Chl-a climatology is included in Figure 3a. See Figure 1 for the box locations.

this bloom that was highlighted by *Perez et al.* [2005]. The second bloom of 2001 coincides with only a modest (1 ms^{-1}) strengthening of zonal winds. Although this wind anomaly is not particularly strong, the anomalously strong secondary bloom of 2001 may be attributed to the low frequency shoaling of the thermocline that amplifies an impact of transient wind events. In distinction from the 2001 event, the second bloom in 2000 does not coincide with local winds, raising the possibility that remote forcing may be partly responsible for the thermocline depth variations in this season, and, thus, for the bloom intensity.

[14] We examine the possibility that wind-forced disturbances in the west are partly responsible for the thermocline depth and Chl-a disturbances in the east by examining the correlation between winds in the west and thermocline depth and Chl-a in the east (Figure 4a). During the secondary bloom season (December–January) we find significant correlations exceeding 0.5 with winds leading thermocline depth by 3 weeks and Chl-a concentration by 4–5 weeks, consistent with the expected delays associated with thermocline adjustment (see Figure S1 in the auxiliary material)[1] and phytoplankton growth [*Longhurst*, 1993]. Although weak wind/SSH correlation at zero lag, the significant wind/SST correlation for the November–December cooling indicates the Bjerknes feedback [*Okumura and Xie*, 2006].

[15] To evaluate the origins of zonal wind fluctuations in the west, we correlate November–December zonal winds in the western box with concurrent winds and mean sea level pressure (MSLP) over the tropical Atlantic and adjacent areas. The spatial structure of correlation pattern for air pressure (Figure 4b) suggests contribution from the two centers of action. The first one locates over the north subtropical high region (that represents the southern pole of the North Atlantic Oscillation that is active in boreal winter). Anomalously high air pressure in the north subtropical high strengthens the northeasterly trades that, in turn, shift the ITCZ south and weaken the southeasterly trades over the equator.

[16] Equatorial zonal winds significantly correlate with anomalous MSLP over the Amazon (Figure 4b). Indeed, the zonal wind and pressure gradient are in balance in the equatorial belt. But, what is of interest is the location of the center of action that sets up an anomalous zonal pressure gradient. It situates itself over equatorial South America, implying that fluctuations of atmospheric pressure produced by disturbances of convection and diabatic heating over the Amazon may affect zonal winds over the equatorial Atlantic.

4. Discussions and Summary

[17] While much of the primary productivity in the tropical Atlantic on seasonal timescales occurs in coastal upwelling zones, significant variability of Chl-a occurs along the equator. In this study, we examine the dynamical processes responsible for the seasonal and interannual variability in this equatorial region, focusing on the 10-year period 1997–2006 covered by observations from the SeaWiFS satellite sensor.

[1] Auxiliary materials are available in the HTML. doi:10.1029/2007GL032466.

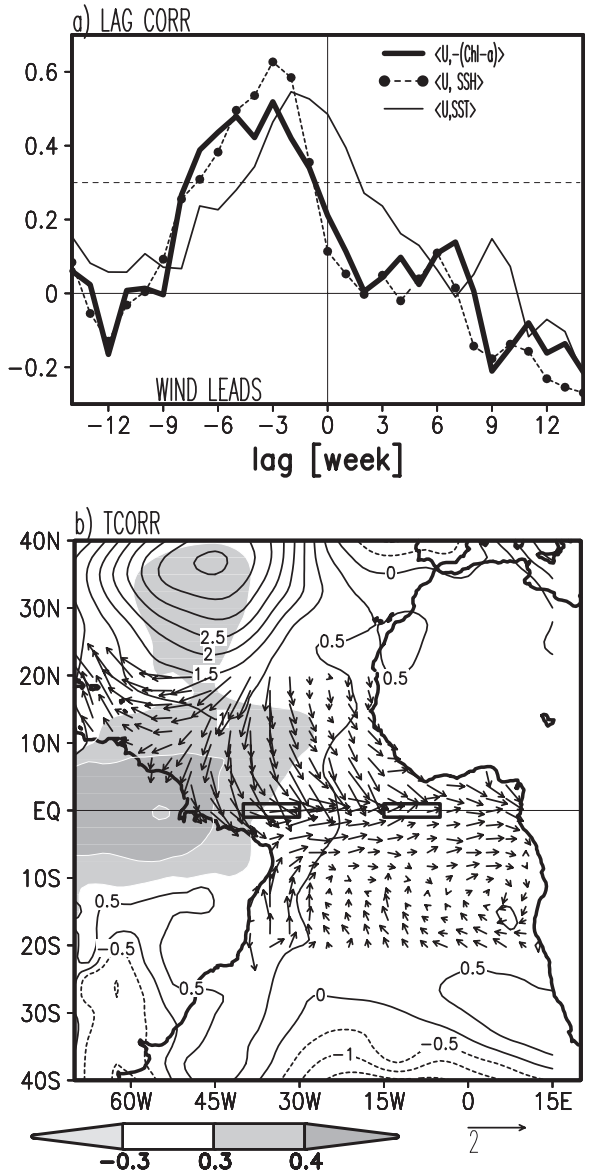

Figure 4. (a) Lagged correlation of anomalous Dec–Jan Chl-a and SSH and Nov–Dec SST in the eastern box with anomalous zonal winds (U) in the western box. Note that Chl-a has been multiplied by (−1). Correlations exceeding ±0.3 are significant at the 99% confidence level. (b) Time regression of anomalous Nov–Dec zonal wind in the western box with anomalous wind velocity and MSLP (contours, mbar/ms^{-1}). Areas where U/MSLP correlation exceeds 0.3 are shaded.

[18] The eastern equatorial region contains a nutrient-limited upwelling regime, so the mixed layer Chl-a is related to thermocline depth. In this region the thermocline shoals twice a year as a consequence of local and remote wind forcing, causing a primary bloom in July–August where Chl-a reaches 0.6 mg.m^{-3} at 0°N, 10°W, and a secondary bloom in December–January where Chl-a reaches 0.3 mg.m^{-3}. Both the primary and secondary blooms are associated with strengthening of the equatorial winds, the former associated with the northward shift of the ITCZ, and the latter associated with the relaxation of the northwest African Monsoon.

[19] Interannual variability of the primary bloom results from the same processes giving rise to interannual variability of SST, that is, fluctuations of the equatorial zonal winds and the consequent thermocline displacement. Like the primary bloom, the secondary bloom is also the result of fluctuations of the thermocline depth, but in contrast to SST, the interannual variability of the secondary bloom is as large as the primary bloom, though its climatological expression is weaker by a factor of two. Indeed, the largest Chl-a anomaly during the 10-year period occurred during the 2001 secondary bloom.

[20] Interannual variability in the eastern equatorial region is the result of the equatorial wind variability. This link explains almost 40% of the thermocline depth variance in the east. The remaining variance is essential and suggests that processes other than instantaneous wind forcing may contribute. Wind anomalies over the western equatorial Atlantic (that trigger vertical displacement of the thermocline) are linked to the atmospheric pressure anomalies over the north subtropical high and over the Amazon. This suggests that equatorial wind anomalies are produced by the meridional displacements of the ITCZ and by anomalies of the Amazon convection.

[21] **Acknowledgments.** We gratefully acknowledge support from the NASA's Oceans Program. The altimeter products are produced by the CLS Space Oceanography Division with support from CNES. QuikSCAT wind is provided by the Seaflux at NASA/JPL.

References

Arnault, S., L. Gourdeau, and Y. Menard (1992), Comparison of the altimetric signal with in situ measurements in the tropical Atlantic Ocean, *Deep Sea Res., Part A*, *39*, 481–499.

Ducet, N., P.-Y. Le Traon, and G. Reverdin (2000), Global high resolution mapping of ocean circulation from TOPEX/Poseidon and ERS-1/2, *J. Geophys. Res.*, *105*, 19,477–19,498.

Gregg, W. W. (2002), Tracking the SeaWiFS record with a coupled physical/biogeochemical/radiative model of the global oceans, *Deep Sea Res., Part II*, *49*, 81–105.

Kalnay, E., et al. (1996), The NCEP/NCAR 40-year reanalysis project, *Bull. Am. Meteorol. Soc.*, *77*, 437–471.

Liu, W. T. (2002), Progress in scatterometer application, *J. Oceanogr.*, *58*(1), 121–136.

Longhurst, A. (1993), Seasonal cooling and blooming in the tropical oceans, *Deep Sea Res., Part I*, *40*, 2145–2165.

McClain, C. R., G. C. Feldman, and S. B. Hooker (2004), An overview of the SeaWiFS project and strategies for producing a climate research quality global ocean bio-optical time series, *Deep Sea Res., Part II*, *51*, 5–42.

Monger, B., C. McClain, and R. Murtugudde (1997), Seasonal phytoplankton dynamics in the eastern tropical Atlantic, *J. Geophys. Res.*, *102*, 12,389–12,412, doi:10.1029/96JC03982.

Morliere, A., and J.-P. Rebert (1972), Étude hydrologique du plateau continental Ivoirien, *Doc. Sci. Cent. Rech. Océanogr. Abidjan*, *3*, 1–30.

Okumura, Y., and S. P. Xie (2006), Some overlooked features of tropical Atlantic climate leading to a new Niño-like phenomenon, *J. Clim.*, *19*, 5859–5874.

Perez, V., E. Fernandez, E. Maranon, P. Serret, and C. Garcia-Soto (2005), Seasonal and interannual variability of chlorophyll-a and primary production in the Equatorial Atlantic: In situ and remote sensing observations, *J. Plankton Res.*, *27*(2), 189–197.

Philander, S. G. H., and R. C. Pacanowski (1986), A model of the seasonal cycle in the tropical Atlantic Ocean, *J. Geophys. Res.*, *91*, 14,192–14,206.

Schott, F. A., J. P. McCreary, and G. C. Johnson (2004), Shallow overturning circulation of the tropical-subtropical oceans, in *Earth Climate: The Ocean-Atmosphere Interaction*, *Geophys. Monogr. Ser.*, vol. 147, pp. 261–304, AGU, Washington, D. C.

Schouten, M. W., R. P. Matano, and T. P. Strub (2005), A description of the seasonal cycle of the equatorial Atlantic from altimeter data, *Deep Sea Res., Part I*, *52*, 477–493.

Servain, J., J. Picaut, and J. Merle (1982), Evidence of remote forcing in the Equatorial Atlantic Ocean, *J. Phys. Oceanogr.*, *12*, 457–463.

Servain, J., A. J. Busalacchi, M. J. McPhaden, A. D. Moura, G. Reverdin, M. Vianna, and S. E. Zebiak (1998), A Pilot Research Moored Array in the Tropical Atlantic (PIRATA), *Bull. Am. Meteorol. Soc.*, *79*, 2019–2031.

Signorini, S. R., R. G. Murtugudde, C. R. McClain, J. R. Christian, J. Picaut, and A. J. Busalacchi (1999), Biological and physical signatures in the tropical and subtropical Atlantic, *J. Geophys. Res.*, *104*, 18,367–18,382, doi:10.1029/1999JC900134.

Uz, B. M., and J. A. Yoder (2004), High frequency and mesoscale variability in SeaWiFS chlorophyll imagery and its relation to other remotely sensed oceanographic variables, *Deep Sea Res., Part II*, *51*, 1001–1017.

J. A. Carton and S. A. Grodsky, Department of Atmospheric and Oceanic Science, University of Maryland at College Park, Computer and Space Science Building 2409, College Park, MD 20742, USA. (senya@atmos.umd.edu)

C. R. McClain, NASA Goddard Space Flight Center, Greenbelt, MD 20771, USA.